Transitions of magnetic configuration at the interface of exchange-coupled bilayers: TbFe/GdFe as a model system

F. Montaigne* and S. Mangin
Laboratoire de Physique des Matériaux, Université H. Poincaré, Boîte Postale 239, F-54506 Vandoeuvre-les-Nancy Cedex, France

Y. Henry
Institut de Physique et Chimie des Matériaux de Strasbourg, CNRS and Université Louis Pasteur, Boîte Postale 43, F-67034 Strasbourg Cedex 2, France

(Received 6 September 2002; published 16 April 2003)

The magnetization profile that forms in the soft part of an exchange-coupled hard/soft bilayer submitted to a rotating in-plane magnetic field has been studied both theoretically and experimentally. The evolution of the stable magnetic configurations as a function of the field orientation has been determined from micromagnetic calculations, for varying strength of the rotating field. The anisotropic magnetoresistance associated with these configurations has been deduced and compared with experimental results obtained on a TbFe/GdFe ferrimagnetic bilayer. A good agreement is obtained between calculated and measured data, without any parameter adjustment. As the applied field is rotated, a twisted magnetization distribution of Bloch type develops in the soft GdFe layer. The simulations show the existence of several possible stable magnetic profiles. These differ either by the amount of magnetization twist only or by the amount of twist and the chirality of the profile. Transport measurements allow one to determine which configuration is actually adopted by the system and in what circumstances the system switches from one configuration to another. Two types of transition are identified. The first one is related to the existence of a hard axis of magnetization in the GdFe layer. The second one corresponds to a change of chirality of the wall.

DOI: 10.1103/PhysRevB.67.144412 PACS number(s): 75.60.Ch, 75.70.−i, 75.30.Et

I. INTRODUCTION

There is currently a great interest for the magnetization reversal properties at the interface of exchange-coupled films. The exchange bias of a ferromagnetic layer is a key point for the development of spin-electronic devices such as magnetic sensors or random access memories.[1,2] Besides the widely studied and used antiferromagnetic/ferromagnetic structure,[3–5] another exchange-coupled film system of interest is the spring-magnet structure.[6] In this system, two ferromagnetic (or ferrimagnetic) layers, a magnetically hard one and a soft one, are ferro- or antiferromagnetically coupled to each other. During the reversal of the soft layer magnetization, a competition between two energies, the Zeeman energy and the exchange interaction, takes place. A magnetic domain wall may be created in the thickness of the layer to decrease the total energy at the interface. Spring magnets thus provide a powerful mean for creating at will and controlling domain walls, and study their behavior under different constraints.[6–8] Well-controlled domain walls are also essential to study another interesting topic still in discussion, that is the magnetoresistance of magnetic domain walls.[9–12]

In the present article, the magnetization configuration of a spring-magnet structure is investigated through its magnetoresistive response in a rotating in-plane magnetic field. The system studied consists of a $Tb_{55}Fe_{45}$ (50 nm)/$Gd_{40}Fe_{60}$ (100 nm) bilayer. In $Gd_{40}Fe_{60}$ and $Tb_{55}Fe_{45}$ ferrimagnetic alloys, the coupling between the Fe and the rare earth spins is antiferromagnetic and the contribution of rare earth moments to magnetization is dominant. Because the exchange coupling between the TbFe and GdFe layers is dominated by Fe-Fe ferromagnetic interactions, the coupling between the net magnetization of the two ferrimagnetic layers is of ferromagnetic nature. The $Tb_{55}Fe_{45}/Gd_{40}Fe_{60}$ system exhibits exchange bias properties.[7] The magnetization of the $Gd_{40}Fe_{60}$ layer, which is magnetically soft, is strongly pinned at the interface by the exchange coupling with the magnetization of the $Tb_{55}Fe_{45}$ layer, which is magnetically extremely hard. As an external field is applied to this system and progressively rotated away from the pinning direction, a Bloch-like domain wall of varying twist may form in the $Gd_{40}Fe_{60}$ layer.

The paper is divided as follows. We first present and discuss the magnetoresistance properties of a single 100-nm thick $Gd_{40}Fe_{60}$ layer in a rotating field. This allows us to extract the intrinsic characteristics of the soft layer and, simultaneously, to introduce the problematic of field-angle-dependent magnetic configuration in the case of a simple system. Then, we focus on the $Tb_{55}Fe_{45}$ (50 nm)/$Gd_{40}Fe_{60}$ (100 nm) spring-magnet structure. A model is developed that shows that several equilibrium magnetization profiles are theoretically possible due to the existence of a uniaxial anisotropy in the soft layer and to the two different chiralities the domain wall can adopt. It is shown that the reversal from one type of profile to another can take place following an irreversible transition from one equilibrium solution to the other. The expected anisotropic magnetoresistance (AMR) signal corresponding to the different profiles is calculated and compared with the results of resistivity measurements performed on the $Tb_{55}Fe_{45}/Gd_{40}Fe_{60}$ bilayer. This permits to conclude on which magnetic profile is really adopted by the system. The dependence of the transitions observed from one magnetic

configuration to another as a function of temperature and field amplitude is presented and discussed in details.

II. EXPERIMENTAL DETAILS

$Tb_{55}Fe_{45}$ and $Gd_{40}Fe_{60}$ alloys were successively deposited on glass substrates by coevaporation of the pure elements from three different sources, in a high vacuum chamber. In the following, these alloys will be referred to as GdFe and TbFe. Prior to their deposition, gold pads were deposited on the substrates (through a mask) and copper test leads were attached to them to eventually ensure very good electrical contacts to the magnetic film. The Gd, Tb, and Fe deposition rates were monitored by quartz microbalances, previously calibrated by optical interferometry. The glass substrates were kept at 77 K during growth in order to obtain amorphous alloys. The pressure in the evaporation chamber was in the 10^{-8} Torr range during deposition. A 30-nm thick capping layer of Si was finally deposited on top of the TbFe/GdFe bilayer to protect it from oxidation. The composition and the amorphous character of the alloys were checked by x-ray analysis and transmission electron microscopy, respectively.

A uniaxial anisotropy in the plane of the film was induced in GdFe by using a specific deposition geometry.[13] Magnetization measurements give a saturation magnetization of $M=(1000\pm100)$ emu/cm^3 and an anisotropy constant of $K=(12\pm2)\times10^4$ erg/cm^3 at 100 K. Further evidence of a well-defined anisotropy in the soft GdFe layer is presented in Sec. III. At temperatures below 100 K, the 50-nm thick TbFe layer is extremely hard magnetically: Its coercive (switching) field is larger than 10 kOe. As a result, its magnetization remains essentially unaffected by the application of external fields as large as 1 kOe.

Electrical resistivity measurements were carried out at temperatures between 12 and 100 K in a continuous flow helium cryostat, using a conventional four-wire method. The resistance of the sample was monitored as the external field **H**, produced by an electromagnet, was continuously rotated in the plane of the film. To avoid induction effects, the angular velocity of the magnet was set to 0.5 deg/s. In these conditions, the angular resolution was found to be better than 0.2 deg. The current was flowing in the plane [current-in-plane (CIP) geometry] and parallel to the easy axis of magnetization (Ox) of the GdFe layer. All the experiments were performed using the same experimental protocol: A saturating field of 12 kOe was first applied at room temperature along the Ox direction. Then the sample was cooled under this saturating field to the measurement temperature. Once this temperature was reached, the field strength was reduced to the required value ($0<H\leqslant1000$ Oe) while its direction was kept unchanged. Finally, resistivity data were taken successively for both counterclockwise and clockwise directions of rotation of the field. This procedure ensured that, at the beginning of each experiment, the magnetization of the soft and hard layers was homogeneously aligned along the easy axis Ox. Note that to make sure that the variations in resistivity observed were solely due to changes in the micromagnetic configuration of the sample, the temperature of the latter had to be stabilized to better than 0.2 K.

III. SINGLE GdFe LAYER

We will first consider the case of a single GdFe film, 100 nm thick, fabricated in the conditions described before. The study of this film will be useful in two ways. First, it will allow us to determine the intrinsic characteristics of the soft layer that is part of the spring-magnet structure under study in this paper. Second, and more important, this study will serve as an introduction to the problematic of field-angle-dependent magnetic configuration in the case of a simple system and, as such, will constitute a reference basis for the description of the behavior of the more complex spring-magnet structure.

A. Model

As already mentioned before and further ascertained in the sequel, the GdFe film possesses a magnetic uniaxial anisotropy in its plane. Let us call its constant K. The evolution of the film magnetization **M**, which may be considered as uniform in an in-plane rotating field **H**, is essentially governed by the Stoner-Wohlfarth Model.[14] In order to obtain theoretically the equilibrium angular position(s) of **M**, $\tilde{\theta}$, one has to find the minima of the total volumic magnetic energy

$$E(\theta)=K\sin^2\theta-HM\cos(\theta-\psi), \tag{1}$$

where θ is the angle between **M** and the easy axis Ox and ψ the angle between **H** and Ox. Equation (1) can be rewritten in a more convenient (dimensionless) manner:

$$\epsilon(\theta)=\frac{1}{2}\sin^2\theta-\frac{H}{H_a}\cos(\theta-\psi), \tag{2}$$

where $\epsilon=E/(H_aM)$ is now the reduced magnetic energy of the system, to be minimized with respect to θ, and $H_a=2K/M$ is the anisotropy field. The system exhibits different behaviors depending on the relative values of H and H_a.

(1) For $H\geqslant H_a$, the energy $\epsilon(\theta)$ admits a single minimum for all ψ. As the field is progressively rotated from 0 to 360°, the magnetization follows more or less closely the field and occupies successively all the possible angular positions θ. In this field regime, there exists an angle-dependent misalignment between **M** and **H**, which writes $\tilde{\theta}-\psi=-\arcsin[H_a/(2H)\sin(2\tilde{\theta})]$. It is zero not only for $\psi=0°$ and 180° ($\mathbf{H}\|Ox$), but also for $\psi=90°$ and 270° ($\mathbf{H}\perp Ox$). For $H=H_a$, its maximum value is 30° (10° for $H=2H_a$). We name this regime A.

(2) For $H_a/2\leqslant H<H_a$, the situation is somewhat more complex. Indeed, the in-plane uniaxial anisotropy, with its twofold symmetry, is responsible for the coexistence, over a certain range of angle ψ centered around 90°, of two energy minima. In the following, these will be called anisotropy wells. Figures 1(a–c) showing the variation of ϵ with θ for $H/H_a=0.6$ and different values of ψ illustrates this property.

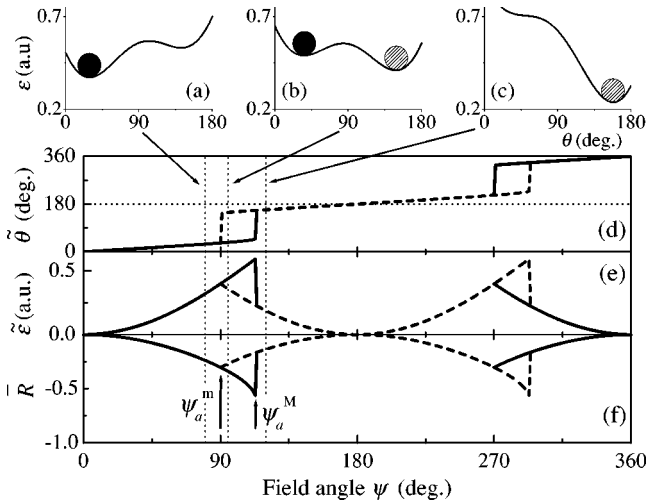

FIG. 1. Results of the model of Sec. III A describing the behavior of a single magnetic layer with homogeneous magnetization in an in-plane rotating field. The reduced field value used is $H/H_a = 0.6$. (a–c) Variation of the normalized energy ϵ [Eq. (2)] as a function of the magnetization angle θ, for different orientation of the applied field: (a) $\psi = 80°$, (b) 95°, and (c) 120°. (d) Possible stable angular positions of the magnetization $\tilde{\theta}$, (e) the corresponding normalized energy $\tilde{\epsilon} = \epsilon(\tilde{\theta})$, and (f) AMR $\bar{R}$, [Eq. (4)] as a function of the field angle ψ. Solid and dashed lines in (d)–(e) correspond to the first and second anisotropy wells, AW1 and AW2, respectively (see text for details).

Here, we will restrict our discussion to the angular range $0 \leqslant \psi < 180°$. What happens for $180 \leqslant \psi < 360°$ may be deduced by symmetry.

Because of the way it is prepared before one starts to rotate the external field, the system initially finds itself in the first anisotropy well AW1, located at $\tilde{\theta}_1 < 90°$ (magnetization closest to the easy direction $\theta = 0°$). The second anisotropy well AW2 located at $\tilde{\theta}_2 > 90°$ (magnetization closest to the easy direction $\theta = 180°$) forms progressively as ψ approaches 90° [Fig. 1(a)]. Its depth increases with increasing ψ but, as long as ψ is less than $\psi_a^m = 90°$, AW2 remains higher in energy than AW1. Beyond ψ_a^m, AW2 gets eventually lower in energy than AW1 and, therefore, it would be energetically advantageous for the system to switch into the magnetic configuration corresponding to AW2. However, to realize this, the system has to overcome the energy barrier that exists between AW1 and AW2 [Fig. 1(b)]. If it is unable to do so, as in the usual Stoner-Wohlfarth model, the system remains in the metastable state corresponding to AW1 until the energy barrier vanishes. This occurs at a certain angle ψ_a^M ($\psi_a^M > \psi_a^m$), beyond which the system necessarily finds itself in AW2 [Fig. 1(c)]. The field regime just described, which we name *B*, is thus characterized by an abrupt change of orientation of **M** [Fig. 1(d)] at an angle ψ such that $\psi_a^m \leqslant \psi \leqslant \psi_a^M$: the system avoids certain angular positions, around $\theta = 90°$ and 270° (hard axis). In this regime B, $\tilde{\theta} = \psi$ only for $\psi = 0°$ and 180° ($\mathbf{H} \| Ox$).

(3) For $H < H_a/2$, a field regime we name C, the two anisotropy wells exist and are separated from each other by an energy barrier, whatever ψ (ψ_a^M does not exist). The system initially located in AW1 can thus only switch to AW2 if a mechanism exists that allows it to pass the energy barrier. In the Stoner-Wohlfarth model, where no such mechanism is considered, the magnetization is ''pinned'' along the easy axis and its angular position just oscillates around $\theta = 0°$ as the external field is rotated.

Our investigations being based on resistivity measurements as a function of the field angle, we need, before proceeding with the analysis of the experimental results, to establish the relationship that exists between the electrical resistance of the system and its magnetic configuration. In the geometry chosen for the reported experiments, we assume that the only source of magnetoresistive effect is the AMR. The GdFe film having a uniform in-plane magnetization and the current flowing through it being parallel to the easy axis Ox its resistance as a function of ψ is given by

$$R(\psi) = R_\perp + \Delta R \cos^2[\tilde{\theta}(\psi)] = R_\parallel - \Delta R \sin^2[\tilde{\theta}(\psi)], \quad (3)$$

where $R_\perp = R(\theta = 90°)$ [respectively, $R_\parallel = R(\theta = 0°)$] is the resistance for a magnetization perpendicular (respectively, parallel) to the current, hence to Ox, and $\Delta R = R_\parallel - R_\perp$. Note that for the GdFe films studied, $R_\parallel$ is larger than $R_\perp$. From Eq. (3), we define the normalized AMR, which will be discussed in the following, as

$$\bar{R}(\psi) = \frac{R(\psi) - R_\parallel}{\Delta R} = -\sin^2[\tilde{\theta}(\psi)]. \quad (4)$$

A normalized AMR of 0 (respectively, -1) thus corresponds to a magnetization parallel (respectively, perpendicular) to the easy axis and current directions. Figure 1(f) shows the normalized AMR curves $\bar{R}(\psi)$ computed using this model, for $H/H_a = 0.6$ (regime *B*). It is worth mentioning that, in regime *B*, the minimum of resistance is reached for the precise angle ψ at which the system switches into the second anisotropy well AW2, irrespective of whether it is allowed to pass the energy barrier between AW1 and AW2 ($\psi_a^m \leqslant \psi < \psi_a^M$) or forced to stay in the metastable state associated with AW1 until the barrier vanishes ($\psi = \psi_a^M$).

B. Experimental results and discussion

The normalized AMR curves $\bar{R}(\psi)$ deduced from the measurements carried out at 100 K on the single GdFe layer, in rotating fields of 200, 500, and 2000 Oe are shown in Fig. 2. The existence of a well-defined uniaxial anisotropy in the GdFe film (with its easy axis parallel to the current) is demonstrated by the twofold symmetry and the dependence on field amplitude of the shape of these curves.

For $H = 500$ and 2000 Oe, $\bar{R}(\psi)$ presents two rather smooth minima, at $\psi = 90°$ and 270°, the level of which ($\bar{R} = -1$) corresponds to the smallest possible AMR value ($R/R_\parallel - 1 = -0.36\%$), expected to be reached when $\tilde{\theta} = \psi = 90°$ or 270°. This clearly shows that the field values of 500 and 2000 Oe belong to regime $A(H \geqslant H_a)$, in which the magnetization passes continuously through all the possible angular positions θ.

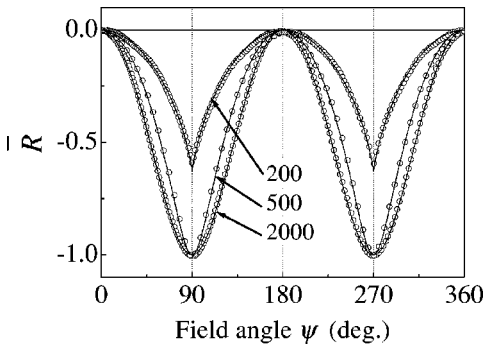

FIG. 2. (Open circles) Normalized AMR curves deduced from measurements at 100 K with applied magnetic fields of 200, 500, and 1000 Oe on a single 100-nm thick $Gd_{40}Fe_{60}$ layer. Solid lines are simulations of the experimental data, using the model of Sec. III A and assuming that the system always adopts its ground state magnetic configuration.

For $H=200$ Oe, the $\bar{R}(\psi)$ curve still exhibits two minima but these are sharp and, more important, higher in value ($\bar{R} \sim -0.6$) than for the two previous field amplitudes. This reveals that the magnetization is never oriented at $\theta=90°$ or 270°, and therefore that H is smaller than H_a (regime B). The fact that the resistivity minima still occur for $\psi=\psi_a^m=90°$ (and 270°), as in regime A, shows that at 100 K the system moves from the first anisotropy well AW1 into the second AW2 as soon as the latter gets lower in energy than the former. It is very likely that thermal agitation is responsible for this phenomena.

Simulations of the experimental resistivity curves $\bar{R}(\psi)$ have been carried out, using the model described in Sec. III A, and assuming that the magnetization always adopts the angular position that corresponds to the absolute minimum of magnetic energy [Eq. (2)]. The only parameter of the model, that is H_a, was fixed to the value of 240 Oe, deduced from superconducting quantum interference device magnetometry. Remarkably, this value allows us to reproduce very closely all of the experimental data (Fig. 2). Then, the Stoner-Wohlfarth model describes well the behavior of the single GdFe film in a given magnetic state. From this model, the height of the energy barrier between the two anisotropy wells can be evaluated. For $\psi=90°$, the equilibrium angular positions of the magnetization are such that $\sin\tilde{\theta}=H/H_a$, from which it follows that the barrier height is simply $\delta(H)=\Delta(H)V=\frac{1}{2}(MH_a)(1-H/H_a)^2V$, where V is the volume of the material susceptible of switching irreversibly from one anisotropy well to the other. Assuming that thermal fluctuations are responsible for the switching at $\psi<\psi_a^M$, which may be the case provided that k_BT is of the order of $\delta(H)/20$ (Ref. 15) or larger, an upper bound for the thermal activation volume may be deduced, which reads $20k_BT/\Delta(H)$. It amounts to 9×10^4 nm^3 (for $H=200$ Oe and $T=100$ K) and is thus much smaller than the volume of the GdFe film studied, which is 4×10^{15} nm^3. This suggests that the change in magnetic configuration occurs by means of a (thermally assisted) nucleation/propagation mechanism, involving the nucleation of a small ''reversed'' nucleus, possibly followed by the subsequent growth of the ''reversed'' fraction of the sample. Furthermore, as is usually the case in imperfect materials, it is all the more likely that nucleation occurs in reality at the location of defects with locally reduced anisotropy field (compared with that of the main phase H_a), hence lowered anisotropy barrier.

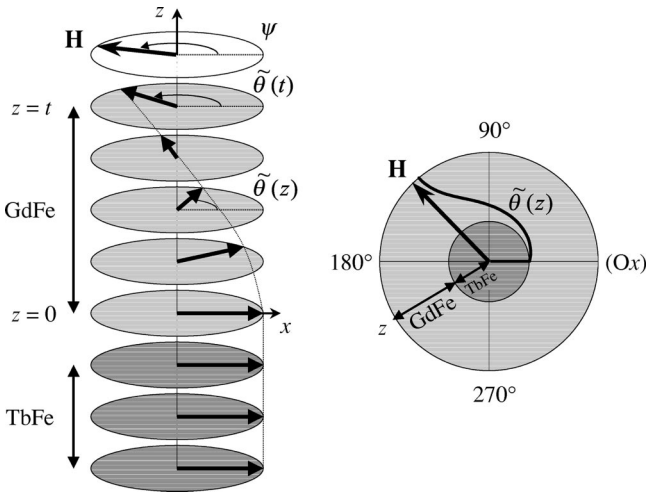

FIG. 3. (Left) Schematic representation of the spin structure forming in the TbFe/GdFe bilayer as the external field **H** is rotated counterclockwise an angle ψ away from the easy axis direction Ox. (Right) Polar plot of the corresponding depth dependence of the magnetization angle $\tilde{\theta}(z)$.

IV. TbFe/GdFe SPRING MAGNET

We now turn our attention to the TbFe/GdFe spring-magnet structure. Its behavior in an in-plane rotating field is of course significantly more complex than that of the single layer described before. In particular, the chirality of the Bloch wall that forms in the soft layer constituting an additional degree of freedom of the system, the magnetic configurations possibly adopted are more numerous.

A. Model

We consider here that, in external fields of moderate amplitude such as those used experimentally, the magnetization of the hard layer is frozen at low temperature due to its very high magnetic rigidity. The TbFe magnetization is homogeneous and aligned along the Ox direction, that is the easy axis of the soft layer, as a result of the cooling procedure described in Sec. II. As a Bloch wall is expected to form in the GdFe layer, its magnetization **M** can no longer be considered as always uniform, as in the case of an isolated layer (Sec. III). Instead, we assume that **M** is (still) laterally invariant but makes an angle $\tilde{\theta}(z)$ with respect to Ox which is depth dependent (Fig. 3). At the TbFe/GdFe interface ($z=0$), the interfacial exchange coupling imposes $\tilde{\theta}(0)=0$. Unless stated otherwise, our discussion will be restricted to equilibrium in-plane magnetization configurations since applied, pinning and demagnetizing fields tend to maintain the

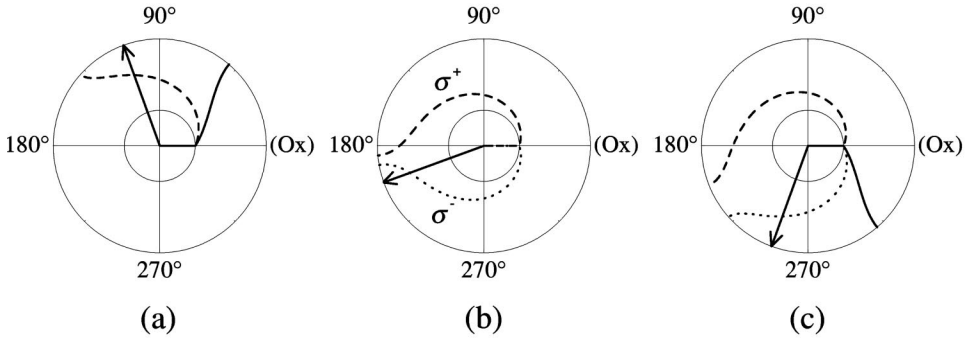

FIG. 4. (a)–(c) Polar plots of the depth dependence of the magnetization angle, as obtained from the model of Sec. IV A. The calculations were carried out for $t/\lambda=4.5$, $H/H_a=0.625$, and several field orientations indicated by arrows: (a) $\psi=110°$, (b) 200°, and (c) 250°. The profiles corresponding to the different local minima of the energy [Eq. (6)] are represented with different line styles.

GdFe magnetization in the plane of the film. This aspect will be further discussed in the last part of the paper.

The surfacic energy of the soft layer is obtained by integrating, over the layer thickness t, the exchange energy characterized by the stiffness constant A, the anisotropy energy of constant K, and the Zeeman energy corresponding to the interaction of **M** with the in-plane external field **H** of angle ψ (measured from Ox):

$$E=\int_0^t\left[A\left(\frac{d\theta(z)}{dz}\right)^2+K\sin^2\theta(z)-HM\cos[\theta(z)-\psi]\right]dz. \tag{5}$$

Equation (5) can be simplified by introducing the exchange length $\lambda=\sqrt{A/K}$ and the anisotropy field $H_a=2K/M$:

$$\epsilon=\frac{E}{\sqrt{AK}}=\int_0^{t/\lambda}\left[\left(\frac{d\theta(\xi)}{d\xi}\right)^2+\sin^2\theta(\xi)-2\frac{H}{H_a}\cos[\theta(\xi)-\psi]\right]d\xi. \tag{6}$$

This allows one to deal with a reduced energy ϵ that contains only two dimensionless parameters t/λ and H/H_a. Notice that, in the figures of this paper, ϵ will systematically be shifted by $-2Ht/(H_a\lambda)$, so that $\epsilon(\psi=0,\theta=0)=0$. In order to determine numerically the magnetic configurations $[\tilde{\theta}(z)]$ that can possibly be (meta)stable in the spring-magnet structure, Eq. (5) was transformed in a discrete form and ϵ was minimized with respect to $\theta(z)$, with the limit condition $\tilde{\theta}(0)=0$. The soft film was thus treated as a chain of spins running normal to the layers.[6] The energy of the chain was minimized iteratively and for every values of ψ, the different local minima the energy ϵ may admit were obtained by starting from different initial conditions.

In order to compare numerical simulations with transport measurements, the AMR of the magnetic profiles minimizing ϵ were also calculated. For a layer with an inhomogeneous magnetization profile and a thickness much larger than the mean free path (a few tenths of nanometers), as the GdFe layer ($t=100$ nm), the total conductance can be considered as equivalent to that of parallel slides of the magnetic material at different depth z, having different magnetization orientation $\tilde{\theta}(z)$ with respect to the current direction, hence different resistivity $\rho(z)$. The sheet resistance R of such a layer is then given by

$$\frac{1}{R}=\int_0^t\frac{dz}{\rho(z)}=\int_0^t\frac{dz}{\rho_\parallel-\Delta\rho\sin^2[\tilde{\theta}(z)]}, \tag{7}$$

where $\rho_\parallel$ (respectively, $\rho_\perp$) is the resistivity for a magnetization homogeneous and parallel (respectively, perpendicular) to the current and $\Delta\rho=\rho_\parallel-\rho_\perp$. As we did for the single layer [Sec. III A, Eq. (4)], we define a normalized AMR as $\overline{R}(\psi)=[R(\psi)-R_\parallel]/[R_\parallel-R_\perp]$, where $R_\parallel=\rho_\parallel/t$ and $R_\perp=\rho_\perp/t$.

Note that the resistance measured on our samples naturally contains a contribution from the TbFe and Si layers. However, the anisotropic magnetoresistance of GdFe is so weak ($\Delta R/R_\parallel\sim 0.3$–$0.4\%$) that the influence of these layers with field-independent conduction on the *normalized* AMR defined above, which is the variable discussed in this paper, is negligible [at first order in $\Delta\rho/\rho_\parallel$, it cancels out as one calculates $\overline{R}(\psi)$].

B. Results and predictions of the model

In the discussion that follows, we will restrict ourselves to the case where the external field is rotated counterclockwise. Upon varying ψ, several energy wells may form depending on the values of t/λ and H/H_a. Of course, these always correspond to minima of the *total* energy of the system. However, in most cases, their origin can be identified as being primarily related to the competition between two of the three energy terms that makes up ϵ [Eq. (6)]. In particular, energy wells may appear, which are primarily determined by the competition between the Zeeman and anisotropy energies. These are equivalent to the two anisotropy wells AW1 ($\tilde{\theta}_1<90°$) and AW2 ($\tilde{\theta}_2>90°$) appearing in the case of the single layer, in regime B [see Sec. III and Fig. 1(b)]. In the case of the spring-magnet structure, we may define the first anisotropy well AW1 as the one corresponding to the magnetic profile with the spins closest to $\theta=0°$ and the second

anisotropy well AW2 as that corresponding to the magnetic profile with the spins closest to $\theta = 180°$ [Fig. 4(a)]. Energy wells may also form which arise primarily from, the competition between the Zeeman and the exchange energies. These are more intimately related to the formation of a Bloch wall in the soft layer. Indeed, as the external field is rotated, a twisted magnetization profile forms in which the spins may rotate either counterclockwise or clockwise, with increasing distance from the hard layer [Fig. 4(b)]. These two possible chiralities of the Bloch wall, which we name, respectively, σ^+ and σ^-, may correspond to two energy wells CW^+ and CW^-, which as we will see in the sequel can possibly coexist under certain conditions. Such a classification of the energy minima in so-called anisotropy and chirality wells is of course arbitrary since a well-identified rightly as being of one kind (say anisotropy) for a given field angle most often transforms progressively in a well of the other kind (chirality) upon increasing continuously ψ. Besides, a few situations exist in which energy wells appear the formation of which does not clearly originate from the competition of two particular energy terms among the three that the total energy ϵ contains; this is especially the case when more than two energy wells coexist [Fig. 4(c)]. However, the classification proposed is particularly convenient to describe the magnetic behavior of our complex system in simple words. This is the reason why we will use it in what follows.

As for the single layer, the behavior of the spring-magnet structure shows different regimes, depending on the value of the controlling parameters t/λ and H/H_a. We shall now illustrate this point. Figure 5 shows the results of the calculations for a normalized thickness of $t/\lambda = 6$ and different values of H/H_a. In each of the four groups of graphs that compose Fig. 5, we have represented, from top to bottom, the angle $\tilde{\theta}(t)$ made by the ''last spin'' of the soft layer, the reduced magnetic energy $\tilde{\epsilon}$ and the normalized AMR $\bar{R}$ of the stable magnetic profiles, as a function of ψ.

(1) Let us first consider the case of a relatively large applied field $H/H_a = 1$ [Fig. 5(a)]. The initial conditions ($\psi = 0$) are such that all the spins are initially aligned along Ox [$\tilde{\theta}(z) = 0$]. This configuration corresponds to the absolute minimum of energy and the maximum resistance of the system ($\bar{R} = 0$). As **H** rotates progressively towards $\psi = 90°$ (counterclockwise), the spins are dragged away from the $\theta = 0°$ direction and a wall with chirality σ^+ starts to develop. This leads to an increase of energy (exchange and anisotropy) and a decrease of resistance. Because the applied field is large, the magnetic profile evolves in a continuous manner (single energy well) in the vicinity of the hard axis ($\psi \sim 90°$). At a certain field angle slightly larger than 90°, the resistance reaches a smooth minimum, which corresponds to the maximum of magnetization perpendicular to the current direction. As **H** rotates further beyond 90° and approaches $\psi = 180°$, the system is in the CW^+ energy well. The energy $\tilde{\epsilon}$ keeps on building up, which is entirely due to an increase in exchange energy, since anisotropy energy now decreases. For $\psi = 180°$, $\tilde{\theta}(t)$ is nearly 180°. However, the resistance is not maximum ($\bar{R} = -0.17$). This feature is the clear signature of the presence of the Bloch wall in the soft layer and the difference in resistance $\bar{R}(0°) - \bar{R}(180°)$ is a direct measure of the amount of magnetization twist in the wall.

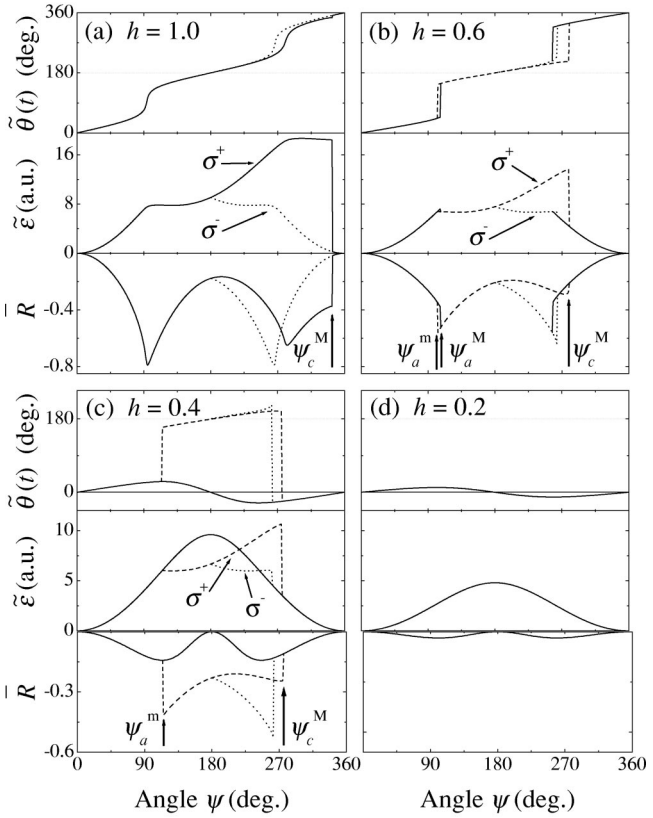

FIG. 5. Results of the model of Sec. IV A, describing the behavior of a spring-magnet structure with $t/\lambda = 6$ in an in-plane rotating field. Four values of the reduced field are considered, which correspond to the four groups of graphs: (a) $H/H_a = 1$, (b) $H/H_a = 0.6$, (c) $H/H_a = 0.4$, and (d) $H/H_a = 0.2$. Represented in each group, as a function of the applied field angle ψ, are the angle $\tilde{\theta}(t)$ made by the last spin of the soft layer (top), the normalized energy $\tilde{\epsilon}$ (middle), and the normalized AMR $\bar{R}$(bottom) of the stable magnetic profile(s). Different line styles are used, which correspond to different local minima of the total energy ϵ [Eq. (6)] (see text for details).

As ψ just exceeds $\psi_c^m = 180°$, the CW^+ energy well [wall with chirality σ^+, Fig. 4(b)] in which the system sits becomes higher in energy than that corresponding to a magnetic profile with a wall of opposite chirality σ^-, that is the CW^- well. However, an energy barrier separates CW^+ and CW^-. From ψ_c^m, the system may thus stay in the metastable σ^+ state or, if a mechanism exists that makes this possible, overcome the energy barrier and fall into the energetically more favorable σ^- state. If the system succeeds in escaping from CW^+, a discontinuous change in magnetic profile occurs ($\sigma^+ \rightarrow \sigma^-$), which allows to reduce the energy $\tilde{\epsilon}$ and unwind the wall upon further rotating the field. If, on the contrary, the system cannot overcome the barrier, the chirality of the wall remains unchanged and the total energy $\tilde{\epsilon}$ and the magnetization twist keep on building up continuously as

ψ increases above ψ_c^m. In this case, the AMR increases until it reaches a maximum at $\psi > \psi_c^m$, then goes through a smooth minimum at $\psi > 270°$, the level of which is higher than that of the first minimum observed close to $\psi = 90°$ (nonequivalent magnetic profiles). Furthermore, the system is forced to stay in the CW^+ well until the barrier vanishes. This eventually occurs for a field angle $\psi_c^M > \psi_c^m$. Beyond ψ_c^M, the system necessarily finds itself in the CW^- well and the chirality of the wall must have changed from σ^+ to σ^- to minimize exchange energy. The discontinuous change in magnetic profile manifests in the $\overline{R}(\psi)$ curve either by a broad pointed maximum if it occurs exactly for $\psi = \psi_c^m = 180°$ or by an abrupt change in resistance if it takes place at $\psi_c^m < \psi \leqslant \psi_c^M$. Note that for reasons of symmetry, the AMR curve is necessarily such that $\overline{R}(\psi) = \overline{R}(360° - \psi)$ after the change of chirality.

In summary, the behavior just described, which belongs to a regime we name *A*, is characterized by a continuous increase of magnetization twist interrupted by an abrupt change of wall chirality at a given angle $\psi_c^m \leqslant \psi \leqslant \psi_c^M$ (where $\psi_c^m = 180°$), followed by a continuous unwinding of the wall.

(2) As the field is reduced to $H/H_a = 0.6$ [Fig. 5(b)], the effect of the uniaxial anisotropy of the soft layer is more pronounced and the magnetization does no longer rotate continuously when the external field is oriented close to the hard axis (ψ slightly larger than 90°). As in the case of the single layer in regime *B*, two anisotropy wells AW1 and AW2 coexist in this angular range. These correspond to magnetic profiles with the same wall chirality σ^+, but different magnetization twists [Fig. 4(a)]. As for the single layer, there exists a field angle ψ_a^m ($\psi_a^m > 90°$ in this case) beyond which the first of these anisotropy wells AW1 gets higher in energy, hence energetically less favorable than the second one AW2, but an energy barrier still separates AW1 and AW2, as well as an angle $\psi_a^M > \psi_a^m$ above which this barrier vanishes. This kind of behavior that belongs to a regime we name also B, by analogy with the case of the single layer, is very similar to the previous one as far as the change of wall chirality is concerned. The main qualitative difference between regime *A* and regime *B* is that the magnetization undergoes a discontinuous change of orientation not only at an angle $\psi_c^m \leqslant \psi \leqslant \psi_c^M$ (change of chirality), as in regime *A*, but also at an angle $\psi_a^m \leqslant \psi \leqslant \psi_a^M$. The passage from AW1 to AW2 gives rise to a sudden drop in resistance and the angle ψ at which this occurs is immediately followed by a sharp minimum in the AMR curve $\overline{R}(\psi)$. Note finally that if the change of chirality occurs before ψ reaches $360° - \psi_a^m$, the AMR curve will also exhibit, at an angle slightly smaller than 270°, an abrupt increase corresponding to the transition of the system from AW2 back to AW1. However, for the sake of simplicity and conciseness, we will not discuss in more details what happens in this case.

(3) If the field is further reduced to $H/H_a = 0.4$ [Fig. 5(c)], the energy barrier between AW1 and AW2 never vanishes (the angle ψ_a^M does not exist anymore). The system can thus escape from AW1 only if a mechanism exists that allows it to overcome the energy barrier. If such a mechanism does not exist, the system is confined in a metastable state (AW1), the twist in the magnetization profile is very limited in amplitude [$\tilde{\theta}(t)$ never reaches 180°] and no discontinuous change is observed in the magnetic profile and $\overline{R}(\psi)$ curve [solid lines in Fig. 5(c)]. In the opposite case [discontinuous lines in Fig. 5(c)], a domain wall of large twist [$\tilde{\theta}(t) \geqslant 180°$] may form and beyond the angle $\psi \geqslant \psi_a^m$ at which it escapes from AW1, the system behaves more or less as in regime *B*. This behavior is part of a regime that, by analogy again, we call *C*.

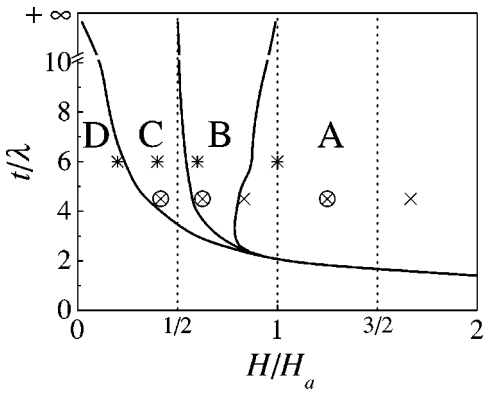

FIG. 6. Calculated phase diagram showing the domain of existence of regimes *A*, *B*, *C*, and *D* as a function of the input parameters t/λ and H/H_a. The stars indicate the simulations of Fig. 5. The crosses correspond to the experimental data of Fig. 8, and the open circles correspond to those experimental data of Fig. 8 that are compared with the model calculations in Fig. 9.

(4) Finally, for the very small field of $H/H_a = 0.2$ [Fig. 5(d)], a single energy well exists (AW1), whatever ψ. The field is so weak that the magnetization cannot be pulled far away from $\theta = 0°$. The system is necessarily in a state similar to the metastable solution of regime *C*. We name this ultimate regime *D*.

Depending on the normalized thickness t/λ, the transition between the different regimes (*A* to *D*) defined before occurs at different fields and all the regimes are not even permitted. Figure 6 shows a calculated phase diagram indicating what regime occurs for a given couple of parameters t/λ and H/H_a. The stars in this phase diagram indicates the four particular cases treated previously ($t/\lambda = 6$, $H/H_a = 0.2$, 0.4, 0.6, and 1). Several aspects of this diagram call for comments. In the limit case of infinite thickness, the influence of the interfacial pinning is of course negligible. Regime *D* is not permitted as the two anisotropy wells AW1 and AW2 exist at very low fields. As expected, the soft layer behaves as if it were an isolated layer with uniaxial anisotropy. When the thickness is reduced, the importance of the interfacial pinning naturally enhances. Its first obvious effect is to prevent the existence of the second anisotropy well AW2, hence the access to it, for the lowest fields (regime *D*). More generally, pinning creates an imbalance between the two easy directions of magnetization and favors AW1 at the expense of AW2. As a result, the field span of regime *B* is reduced: regime *A* extends on this side of H_a and regime *C* extends beyond $H_a/2$. Finally, for the smallest thicknesses ($t/\lambda \leqslant 2$ typically), pinning (exchange) strongly prevails over anisot-

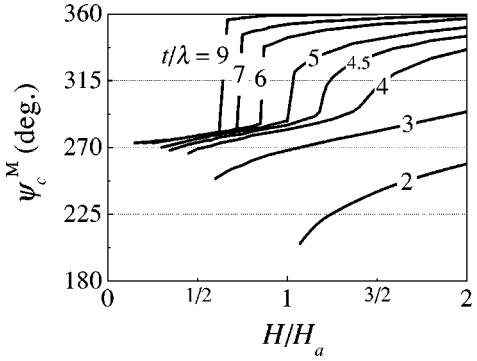

FIG. 7. Calculated evolution of the critical angle of chirality reversal ψ_c^M as a function of the reduced field H/H_a, for various normalized thicknesses t/λ of the soft layer.

ropy. As a consequence, regimes *B* and *C* do not exist and a direct transition exists from regime *A* to regime *D*.

We have shown that in regimes *A* and *B*, and also in regime *C*, if the system can escape from AW1, which we will assume in the rest of this section, a counterclockwise (σ^+) magnetic spiral forms in the soft layer when the applied field is rotated counterclockwise. As the rotation passes $\psi_c^m = 180°$, it becomes energetically more favorable to have a clockwise (σ^-) twist of the soft layer magnetization. However, unless a mechanism exists that allows it to overcome the energy barrier existing between these two configurations, the system cannot adopt immediately the less energetic σ^- magnetization profile. It can only do so at a certain critical angle ψ_c^M for which the energy barrier vanishes. Figure 7 shows the variation of this critical angle as a function of the reduced field H/H_a, for different normalized thicknesses t/λ of the soft layer. Depending on the values of t/λ and H/H_a, the change of chirality at ψ_c^M is driven and determined by qualitatively different mechanisms. We shall discuss this now.

(1) For small thicknesses (and large fields necessarily), the domain wall extends over the entire film thickness. The rotating field drags the spins in the soft layer rather far away from $\theta = 0°$. However, as long as $\psi < \psi_c^M$, these lag in orientation well behind the field. As an illustration, the angle of the topmost spin $\tilde{\theta}(t)$ is only 180° when $\psi = 200°$, for $t/\lambda = 3$ and $H/H_a = 1$. The total energy of the system is thus dominated by the exchange and the Zeeman contributions. The change of chirality then occurs to reduce simultaneously these two energy terms of comparable importance.

(2) In the case of large thicknesses ($t/\lambda > 4$) and low fields, it is anisotropy that primarily determines the critical angle ψ_c^M. The behavior of the spring-magnet may be schematized as follows. As ψ approaches 270° (hard axis), the system is in the second anisotropy well AW2 and many of the "soft" spins are oriented such that $180° \leqslant \tilde{\theta}(z) < 360°$. As ψ gets larger than 270°, anisotropy tends to make these spins switch (irreversibly) back towards the $\theta = 0°$ direction (AW1 well). If this occurred by further rotating the spins counterclockwise, i.e., without a change of the wall chirality, this would result in a dramatic increase of exchange energy. To avoid this, the switching from AW2 to AW1 must necessarily be accompanied by a $\sigma^+ \rightarrow \sigma^-$ transition. In this regime, the change of chirality is therefore directly related to the stability of the second anisotropy well AW2. This is the reason why the critical angle is of order 270° and is not very sensitive to the soft layer thickness.

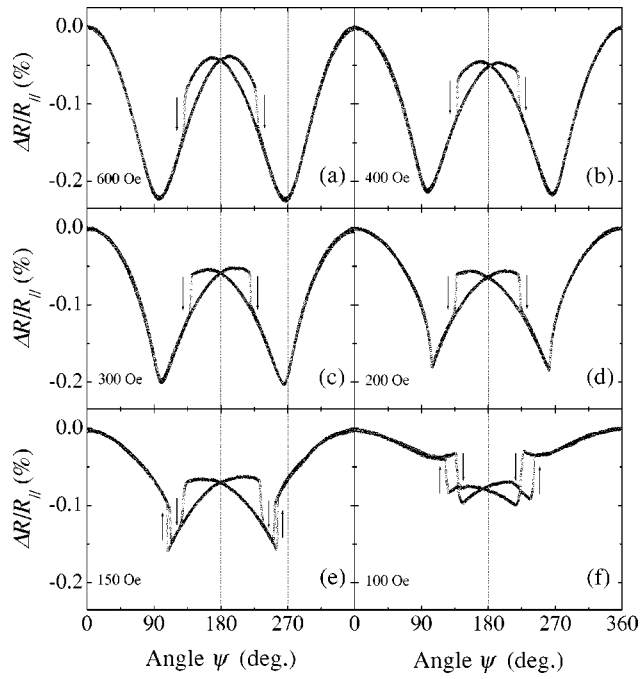

FIG. 8. Magnetoresistance ratio $\Delta R/R_{\parallel} = R(\psi)/R_{\parallel} - 1$ vs field angle ψ, as deduced from the measurements carried out at 50 K on a $Tb_{55}Fe_{45}$ (50 nm)/$Gd_{40}Fe_{60}$ (100 nm) spring-magnet structure. The magnitude of the rotating field is indicated next to the curves.

(3) For large thicknesses and fields, there is no switching from one anisotropy well to the other anymore and the domain wall would go on winding continuously if this did not lead to an excessive exchange energy. Then, in this case, the $\sigma^+ \rightarrow \sigma^-$ transition essentially occurs to release exchange energy. As in our model the change of chirality necessarily proceeds by unwinding of the domain wall (which will be described in more details later), the value of ψ_c^M is determined by the competition between the exchange energy that is reduced and the Zeeman energy that increases as the spins align parallel to the direction of the hard layer magnetization, during this process. The Zeeman energy rising with increasing applied field, the predicted variation of ψ_c^M with H is a monotonous increase.

C. Experimental results and discussion

Figure 8 shows examples of AMR curves recorded at 50 K on the $Tb_{55}Fe_{45}$ (50 nm)/$Gd_{40}Fe_{60}$ (100 nm) bilayer by rotating the external field successively counterclockwise and clockwise. Several characteristic features of these curves clearly indicate the formation of a twisted magnetization profile in the soft layer upon rotation of **H**. First, the minima in the AMR curves never occur at 90° and 270° (**H** parallel to the hard axis), whereas they systematically do so in the case of a single GdFe layer (Sec. III B). Second, the level of resistance reached when the field is oriented at $\psi = 180°$ is

significantly lower than that measured at the very beginning of the rotation ($\psi=0°$), that is, for a state in which the GdFe magnetization distribution is without fail uniform. Third, the (local) maxima of resistance observed about half way through the counterclockwise (respectively, clockwise) AMR curves are systematically shifted towards larger (respectively, smaller) angles with respect to the position where they appear for the single layer, that is, $\psi=180°$. Last, even at fields much larger than the GdFe anisotropy field $H_a=240$ Oe [Figs. 8(a, b)], the experimental curves exhibit rotational hysteresis and abrupt, irreversible changes in resistance. No such changes being expected, neither observed, for a soft layer of uniform magnetization, these can undoubtedly be attributed to a change of chirality of the wall formed in the GdFe layer.

Most of the regimes evoked in Sec. IV B are represented in the AMR curves of Fig. 8 (see Fig. 6). Those of Figs. 8(a–c) ($H/H_a=2.50$, 1.67, 1.25) show deep minima and a continuous variation of resistance in the vicinity of the hard axis, which are characteristic of regime *A*. Curves of Fig. 8(e) ($H/H_a=0.63$) exhibit sharp minima immediately preceded or followed by abrupt changes in resistance, which are characteristic of regime *B*, while those of Fig. 8(d) ($H/H_a=0.83$) correspond almost exactly to the boundary between regime *A* and regime *B* [Fig. 6]. Finally, the AMR curves of Fig. 8(f) ($H/H_a=0.42$), with their abrupt drops of resistance preceded by flat regions (or very shallow minima), are emblematic of regime *C*. Interestingly, the data of Fig. 8(f) reveal the formation of a wall of large twist [$\overline{R}(180°) < \overline{R}(0°)$], even in that low field regime where the energy barrier between AW1 and AW2 never vanishes theoretically. Obviously, this barrier is overcome. Note finally that the experimental setup used did not have the thermal stability required to observe regime *D*. In this regime indeed, the AMR response of the sample studied was similar in amplitude as the changes in resistance induced by temperature fluctuations as small as 0.1–0.2 K.

Except for the features related to the chirality reversal, the normalized AMR curves do not show large global changes with varying temperature. Their amplitude and shape remain almost the same, for a given field value. Furthermore, the transition from regime *A* to regime *B*, which, as we have seen before, clearly manifests by the appearance of sudden resistance jumps in the vicinity of the hard axis direction, is found to occur always for *H* slightly smaller than 200 Oe, irrespective of the temperature. This reveals that the anisotropy field H_a and the exchange length λ do not vary greatly between 12 and 100 K.

Once again for the sake of simplicity, we will from now onwards restrict our discussion to the experimental data obtained with the field rotated counterclockwise. Figure 9 compares normalized AMR curves $\overline{R}(\psi)$ deduced from the measurements at 50 K with simulations. For this comparison limited to few field values, the experimental data were chosen so that each of the regimes *A* [Fig. 9(i)], *B* [Fig. 9(f)], and *C* [Fig. 9(c)] be represented (see Fig. 6). The simulations were performed with $H_a=240$ Oe (see Sec. III B). To get an estimate of the exchange stiffness *A* in the GdFe layer, we used the exchange constants J_{GdGd}, J_{GdFe}, and J_{FeFe} reported by Hansen and co-workers,[16] the interatomic distances given by Cargill,[17] and the formula established by Hasegawa[18] and Mimura *et al.*[19] that relates *A* to the aforementioned parameters in the case of ferrimagnetic amorphous alloys. We obtained $A=6\times10^{-7}$ erg/cm, from which we deduced $\lambda=\sqrt{A/K}=22$ nm (using $K=1.2\times10^5$ erg/cm^3, see Sec. II), and ultimately $t/\lambda=4.5$. The only parameter that was adjusted so as to get the best possible agreement between theory and experiment is the value of $R_\perp$ for the bilayer (see Sec. IV A), a parameter not accessible experimentally but necessary to work out the normalized AMR $\overline{R}$ from the experimental data.

Figures 9(f, i) illustrates the fact that, with the immediately noticeable exception of the chirality reversal angle, calculated data can reproduce experimental ones rather closely. Thus, our model (Sec. IV A) seems successful in determining the stable configurations of the magnetization before and after the $\sigma^+\rightarrow\sigma^-$ transition. This agreement is also a strong support of our assumption that the magnetization twist does not penetrate significantly into the hard TbFe layer, for the applied field amplitudes used in this work ($H\leqslant1000$ Oe).

At very small fields, however [Fig. 9(c)], the experimental AMR data deviate significantly from the theoretical ones in a narrow range of field angle extending approximately from ψ_c to the sharp resistance increase associated with the AW2 $\rightarrow$AW1 transition [$\psi\sim245°$ in Fig. 9(c)]. This deviation is found to get stronger and stronger as the temperature and/or the field is reduced. Simultaneously, the resistance jump corresponding to the $\sigma^+\rightarrow\sigma^-$ transition becomes more and more ill-defined. In the angular range discussed, the system does no longer behave as a single chain of spins and the MR curve lies somewhere in between that predicted for a σ^+ wall [dashed line in Fig. 9(c)] and that predicted for a σ^- wall [dotted line in Fig. 9(c)]. This suggests that lateral inhomogeneities in the magnetization distribution of the GdFe layer form as the system engages in the change of wall chirality and that, subsequently, domains of opposite chiralities coexist in the GdFe layer.

Whatever be the temperature and the field amplitude, the AMR curve does not show a pointed maximum at $\psi=\psi_c^m=180°$. Instead, $\overline{R}(\psi)$ keeps on rising towards a smooth maximum, generally located far beyond $\psi_c^m=180°$. This shows clearly that the change of wall chirality does not take place at ψ_c^m, i.e., immediately after the CW$^+$ energy well got lower in energy than CW$^-$. A comparison of the experimental and calculated data [Figs. 9(c, f, i)] reveals, however, that the transition occurs well before ψ_c^M, that is, the angle at which the energy barrier between CW$^+$ and CW$^-$ vanishes theoretically. From these observations, it follows that the spring-magnet system remains for a long-time prisoner of the metastable σ^+ state, but yet escapes from it at an angle such that $\psi_c^m<\psi<\psi_c^M$. Moreover, transport measurements confirm that it is possible to create, in TbFe/GdFe spring-magnet structures, Bloch walls with a twist larger than 180° (Fig. 9), a result already obtained from polarized neutron reflectometry.[20] As expected from our model, the AMR

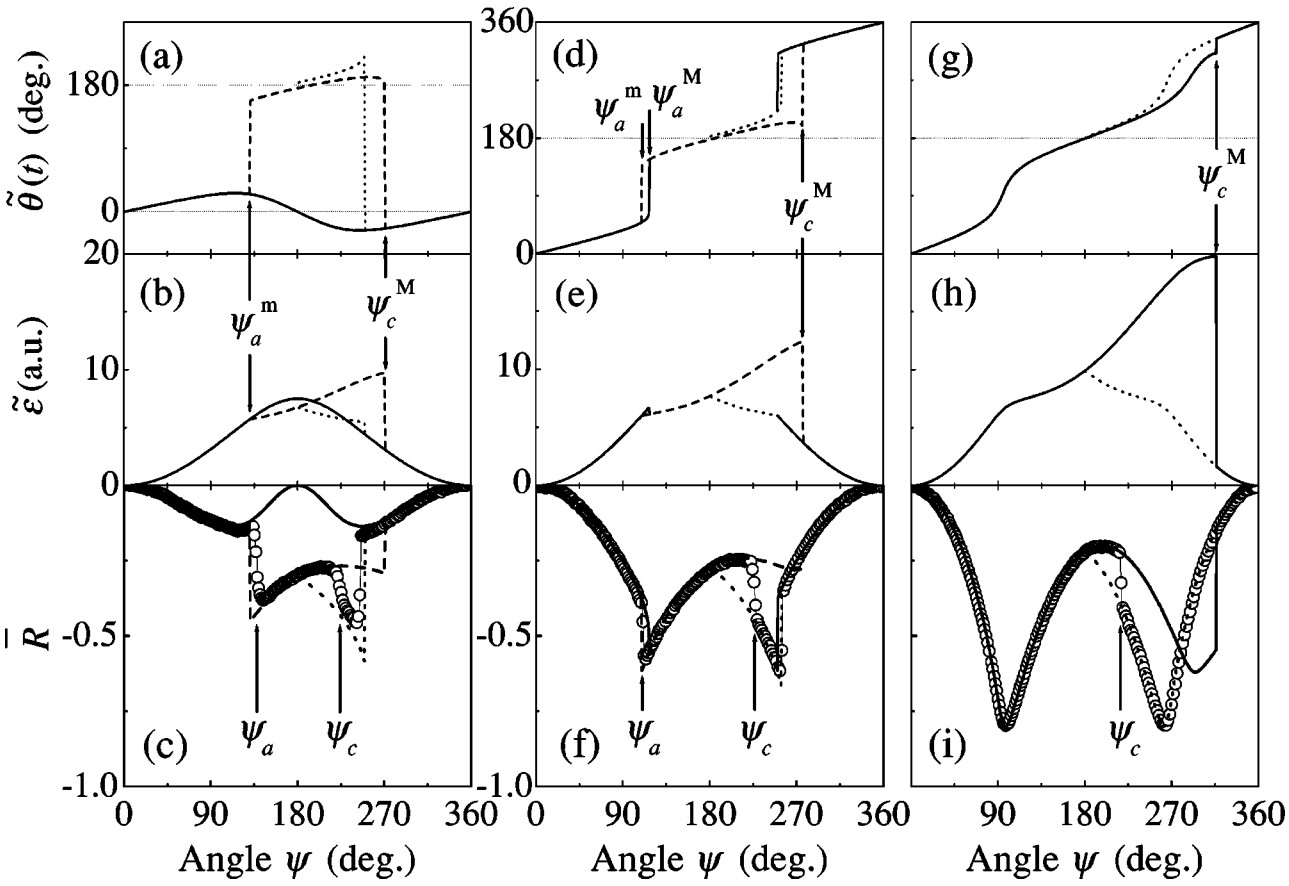

FIG. 9. (c, f, i) Comparison between $\bar{R}(\psi)$ curves deduced from the experiments per-formed at 50 K on a $Tb_{55}Fe_{45}$ (50 nm)/ $Gd_{40}Fe_{60}$ (100 nm) spring-magnet structure (open circles) and the results from the model of Sec. IV A (lines), assuming $t/\lambda = 4.5$ and $H_a = 240$ Oe, for three different field values: (c) $H = 100$ Oe, (f) $H = 150$ Oe, and (i) $H = 300$ Oe, corresponding to regimes *C*, *B*, and *A*, respectively. Also represented are the corresponding theoretical angular variations of the angle $\tilde{\theta}(t)$ (a, d, g) and of the energy $\tilde{\epsilon}$ (b, e, h) associated with the stable magnetic profile(s) of the soft layer. As in Fig. 1, different line styles are used, which correspond to different local minima of the energy ϵ [Eq. (6)].

curves obey the symmetry relationship $\bar{R}(\psi) = \bar{R}(360° - \psi)$, for $\psi > \psi_c$, in regime *A* [Fig. 9(i)].

Figure 10 shows the variation of the angular position of the first AMR minima, ψ_a, as a function of the field strength, together with those expected from the model for the particular angles ψ_a^m (regimes *B* and *C*, $89 \leqslant H \leqslant 192$ Oe) and ψ_a^M (regime *B*, $137 \leqslant H \leqslant 192$ Oe) defined in Sec. IV B. One may immediately notice that ψ_a coincides rather well with ψ_a^m in both regimes *B* and *C*. Thus, we can conclude that, as the single soft layer, the spring-magnet system rapidly minimizes its energy as ψ exceeds ψ_a^m by switching from the more energetic anisotropy well AW1 to the less energetic AW2. Therefore, there exists also for the spring-magnet a mechanism that makes it possible to pass the energy barrier between AW1 and AW2 and escape from metastable AW1. At 100 K, the agreement between ψ_a and ψ_a^m is perfect. At lower temperatures, however, ψ_a is systematically larger than ψ_a^m (though it does reach ψ_a^M, in regime *B*). Furthermore, ψ_a increases with decreasing temperature and the difference $\psi_a(T) - \psi_a^m$ increases with decreasing field. These observations are consistent with a thermally activated transition from AW1 to AW2. The height of the energy barrier between AW1 and AW2 cannot be obtained in a simple analytical manner, as in the case of the single GdFe layer (Sec. III B) and its evaluation is beyond the scope of the present work. However, even if this barrier height proved strongly reduced, as compared to the case of the single GdFe layer, it

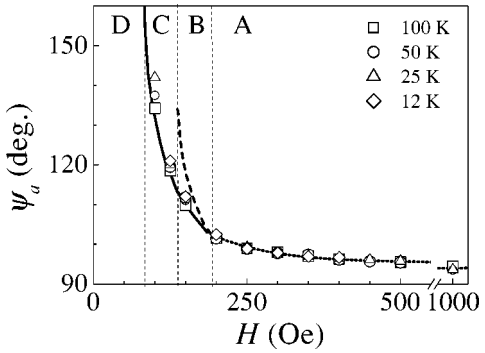

FIG. 10. (Symbols) Experimental variation of the angular position of the first AMR minimum ψ_a ($90° < \psi_a < 180°$) as a function of the applied field amplitude for various temperatures: (□) 100 K, (○) 50 K, (△) 25 K, (◇) 12 K. (Lines) Results from the model calculations. The solid line (regimes *B* and *C*) and the dashed line (regime *B*) correspond to the field variations of the particular angles ψ_a^m and ψ_a^M, respectively (see text for details).

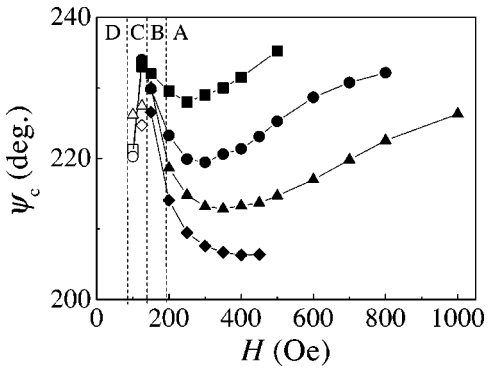

FIG. 11. Experimental variation of the angle of chirality reversal ψ_c as a function of the applied field amplitude, for various temperatures: (squares) 100 K, (circles) 50 K, (triangles) 25 K, (diamonds) 12 K. The lines are guides to the eye.

can be ascertained that the corresponding thermal activation volume upper bound (see Sec. III B), though increased, would still remain many orders of magnitude smaller than the total volume of the soft layer. Therefore, here again, a nucleation-propagation mechanism (possibly defect assisted) is certainly implicated in the AW1→AW2 transition.

Finally, it must be noticed that, in regime $A(H \geqslant 192$ Oe), ψ_a follows perfectly the field variation predicted by the model. With increasing field, ψ_a tends asymptotically towards 90°. This corresponds to the increasingly large compression of the Bloch wall against the hard TbFe layer.[7]

Figure 11 presents the experimental variation of the critical angle ψ_c as a function of the field amplitude, for various temperatures. Contrary to that of ψ_c^M (Fig. 7) determined from our model, the field variation of ψ_c is not monotonous. With increasing field, it first shows a rapid increase in a field range corresponding approximately to regime *C*, then a maximum close to the boundary between regime *C* and regime *B*, followed by a steep decrease leading to a broad minimum at $H_m = 250$–400 Oe (depending on the temperature), which is somewhere in regime *A*, and finally a slow increase at large field values. Concomitantly, the abruptness of the transition varies also in a nonmonotonous manner, and appears as maximum at H_m (Fig. 8). Then, in addition to the fact that it cannot predict the correct value of the critical angle ψ_c, our one-dimensional model is also unable to account qualitatively for the complex field behavior of ψ_c. As already mentioned, this model allows only one mode of chirality reversal. This is the unwinding mode in which the spins remain in the plane of the layers: the spiral profile unwinds so that the spins get parallel to the pinning direction and then it winds in the opposite direction. The incapacity of the model used to reproduce, even qualitatively, the experimental variation of ψ_c suggests that different processes of chirality reversal might occur in our spring-magnet structures depending on the field strength. One may notice, however, that those data points located on the lower field side of the sharp maximum in the field variation of ψ_c (open symbols in Fig. 11) correspond precisely to those temperature and field values for which a clear deviation is observed, beyond ψ_c, between the experimental and the calculated MR data [see Fig. 9(c)]. This is an indication that the occurrence of the maximum in the $\psi_c(H)$ curve could in fact be related to the formation, at small fields, of a multidomain structure in the soft layer, rather than to a real change of chirality reversal process.

Another still open question relates to the temperature dependence of ψ_c at large fields. Trivially, one would expect thermal agitation to help in the jumping of the energy barrier that separates CW^+ and CW^-, as it helps to pass one separating AW1 and AW2, and therefore to give rise to a decrease of ψ_c with increasing temperature. Unexpectedly, ψ_c is found to behave in the opposite way, that is to increase continuously with rising temperature. This shows that, if thermal activation plays a role in the determination of ψ_c, this role is either minor or nontrivial. On the other hand, it seems unlikely that the rather large thermal variation of ψ_c observed be (entirely) ascribable to a variation with temperature of the intrinsic magnetic parameters of the system, namely, the exchange length and anisotropy field. Although variations of λ and H_a cannot be excluded, these must necessarily be small, since as already mentioned before, the angular AMR response of the TbFe/GdFe bilayer is globally unchanged in the temperature range investigated and no variation of these controlling parameters had to be introduced in the model in order to simulate successfully the AMR curves recorded at different temperatures. Furthermore, if some variations of H_a were responsible for the observed behavior, their effect should diminish, hence the $\psi_c(H)$ curves corresponding to different temperatures should tend to merge as the amplitude of the external field increases. This is in contradiction with the experimental observations (Fig. 11).

What has not been considered so far is the possibility to have a magnetization oriented out of the plane, at least during the chirality reversal. Our one-dimensional model can readily be modified to include this possibility: The total surfacic energy of the system has to be rewritten as

$$E = \int_0^t \left[A\left(\frac{d\theta}{dz}\right)^2 \cos^2\varphi + A\left(\frac{d\varphi}{dz}\right)^2 - K\cos^2\theta\cos^2\varphi - MH\cos(\theta-\psi)\cos\varphi + 2\pi M^2 \sin^2\varphi \right] dz, \qquad (8)$$

where φ denotes the angle of the magnetization with respect to the plane of the film. This energy being an even function of φ, the in-plane configuration, solution of Eq. (5), remains an equilibrium solution of Eq. (8). *A priori*, this in-plane configuration may get unstable if the decrease of exchange energy following a reorientation of the magnetization out of the plane is larger than the concomitant increase in demagnetizing energy. However, a reversal mode involving such a reorientation was not found numerically for the set of parameters (M, A, K) describing the system studied.

The chirality reversal of a Bloch-like wall has also been studied recently, by means of torque magnetometry, in exchange-spring magnets consisting of epitaxial SmCo (20 nm)/Fe (5–50 nm) bilayers, by Platt and co-workers.[21] The range of external field amplitude considered by these authors (1–12 kOe) is, however, different from that investigated in

the present work (0.1–1 kOe) since it is much closer to the field beyond which the hard layer irreversibly switches its magnetization. As a result, the magnetization distribution of the hard SmCo layer could not be considered as unaffected by the applied rotating field since the magnetization twist penetrates significantly in it. Maybe due to this difference in the experimental conditions, the thermal and field behaviors of the critical angle found by Platt *et al.* are completely unlike those we report here: ψ_c increases with decreasing temperature and exhibits a maximum in its variation with the external field amplitude. Interestingly, using three-dimensional micromagnetic simulations, the authors have shown the existence of another possible mode of reversal of the wall chirality, named the fanning mode. Contrary to the unwinding mode, the fanning mode is a localized mode: the micromagnetic structure of the film is not laterally invariant during the reversal.[22] In this new mode, the spiral structure of the magnetization distribution is maintained during the reversal and the spins fan out of the plane, thus avoiding the large Zeeman energy enhancement that accompanies the wall unwinding. This mode is characterized by a decrease of the critical angle with increasing external field and is energetically more favorable than the unwinding mode at large fields. The occurrence of a transition from the unwinding mode at small fields to the fanning mode at large fields has thus been proposed by Platt *et al.* as a possible explanation for the nonmonotonous field variation of ψ_c, in SmCo/Fe bilayers.

In our case, a similar explanation does not hold and, for obvious energetic reasons, the fanning mode cannot be evoked to account for the field variation of ψ_c below H_m. Furthermore, it is important to note that although the model calculations of Ref. 21 allowed the authors to reproduce qualitatively the field behavior of ψ_c for the SmCo/Fe system, the calculated values of the critical angle are, like in our case (where $\psi_c < \psi_c^M$), systematically greater than the values deduced from the experiments. As Platt and co-workers, we believe that the reason for this is that more complex phenomena are implicated in the chirality reversal. In particular, defects might also play a major role in this process, especially at small fields. It is likely that, as for the anisotropy well transition, the chirality reversal occurs in reality through the (also possibly thermally activated) nucleation of a small reversed nucleus in a favorable region of the soft film, followed by the subsequent growth of the reversed fraction of the sample.

In order to improve our understanding of the chirality reversal process, we are currently performing after-effect measurements designed to look at the dynamics of this process and numerical calculations of the height of the intrinsic energy barrier that must be overcome. The results of these investigations will be the subject of a future paper.

V. CONCLUSION

Magnetotransport measurements, in the CIP geometry, have been used to study the twisted magnetization profile forming in the soft GdFe layer of a TbFe/GdFe spring-magnet structure, as a rotating external field of moderate amplitude is applied to it. The experimental observations have been explained by considering the anisotropic magnetoresistance changes associated with the progressive winding and unwinding of this spiral profile. Experimental data have been modeled using a simple one-dimensional micromagnetic model in which the hard TbFe layer magnetization is supposed to be frozen and the soft GdFe layer is treated as a chain of spins running normal to the TbFe/GdFe interface. A good agreement found between the experiment and the simulation confirms our postulate that AMR is the main source of magnetoresistance in the ferrimagnetic TbFe/GdFe hard/soft structure. If a domain wall magnetoresistance effect associated with the presence of the Bloch-like wall exists in this structure, it is very weak compared to AMR, as already observed in similar systems.[23]

The model calculations have shown the coexistence, in certain ranges of field angle, of several possible magnetization profiles corresponding to local minima of the total energy of the magnetic system, containing exchange, Zeeman, and (uniaxial) anisotropy contributions. These profiles may differ by the amount of magnetization twist only or by the amount of twist and the chirality of the helical profile. In the first case, the energy wells find essentially their origin in the competition between the Zeeman and anisotropy energies (anisotropy wells), whereas in the second case, they arise mainly from the competition between the Zeeman and exchange terms (chirality wells). Experiments have allowed us to determine in what energy well the system actually finds itself for a given field angle and in what circumstances it passes irreversibly from one magnetic configuration to another. For the anisotropy well transition that exists solely at relatively small fields and occurs as the field is oriented close to the soft layer hard axis, it has been found that the system rapidly minimizes its energy by switching almost immediately from the more energetic metastable state to the ground state, despite the energy barrier that, according to our model, separate the two anisotropy wells. Indications have been given that this transition is thermally activated. In contrast, the chirality reversal has been shown not to occur as soon as the chirality well the system occupies gets metastable. Yet, this transition happens well before the energy barrier that separates the two chirality wells vanishes. The critical angle at which the wall chirality reverses has been shown to exhibit peculiar and still unexplained field and temperature behaviors.

Finally, we wish to emphasize again the fact that the TbFe/GdFe ferrimagnetic system studied in this work is in many respects similar to the usual antiferromagnetic/ferromagnetic (AF/F) layered heterostructures. In particular, the TbFe/GdFe system shows exchange bias at low temperature. In our system, the magnetic configuration at the interface is, however, a simple Bloch wall, as suggested by Mauri and co-workers,[24] whereas in AF/F structures it can be significantly more complex.[25] The present paper demonstrates that angle-dependent magnetotransport measurements can provide precious insights into the magnetic configuration at the interface of exchange-coupled ferrimagnetic bilayers. They could just as well do so for AF/F structures. They might help in clarifying whether or not magnetic domain

walls form in the ferromagnetic components of these structures, a possibility sometimes suggested to explain (1) the inability for most of the models of exchange bias to correctly predict the magnitude of the bias field and (2) the unexpected appearance of exchange bias at a magnetically compensated AF interface.[25]

ACKNOWLEDGMENTS

The authors thank M. Hehn, A. Schuhl, and B. Barbara for fruitful and pleasant discussions, S. Fonfrede for help with the numerical calculations, L. Joly, F. Mouginet, and D. Pierre for help with experiments.

*Electronic address: montaigne@lpm.u-nancy.fr

[1] D. Wang, M. Tondra, J.M. Daughton, C. Nordman, and A.V. Pohm, J. Appl. Phys. **85**, 5255 (1999).

[2] S.S.P. Parkin *et al.*, J. Appl. Phys. **85**, 5828 (1999).

[3] A.E. Berkowitz and K. Takano, J. Magn. Magn. Mater. **200**, 552 (1999).

[4] J. Nogues and I.K. Schuller, J. Magn. Magn. Mater. **192**, 203 (1999).

[5] M. Kiwi, J. Magn. Magn. Mater. **234**, 584 (2001).

[6] E.E. Fullerton, J.S. Jiang, M. Grimsditch, C.H. Sowers, and S.D. Bader, Phys. Rev. B **58**, 12 193 (1998), and references therein.

[7] S. Mangin, G. Marchal, and B. Barbara, Phys. Rev. Lett. **82**, 4336 (1999).

[8] K.V. O'Donovan, J.A. Borchers, C.F. Majkrzak, O. Hellwig, and E.E. Fullerton, Phys. Rev. Lett. **88**, 067201 (2002).

[9] G. Tatara and H. Fukuyama, Phys. Rev. Lett. **78**, 3773 (1997).

[10] J.-E. Wegrowe, D. Kelly, A. Franck, S.E. Gilbert, and J.-Ph. Ansermet, Phys. Rev. Lett. **82**, 3681 (1999).

[11] U. Ebels, A. Radulescu, Y. Henry, L. Piraux, and K. Ounadjela, Phys. Rev. Lett. **84**, 983 (2000).

[12] R. Danneau, P. Warin, J.P. Attané, I. Petej, C. Beigné, C. Fermon, O. Klein, A. Marty, F. Ott, Y. Samson, and M. Viret, Phys. Rev. Lett. **88**, 157201 (2002).

[13] S. Mangin, C. Bellouard, G. Marchal, and B. Barbara, J. Magn. Magn. Mater. **165**, 161 (1997).

[14] E.C. Stoner and E.P. Wohlfarth, Philos. Trans. R. Soc. London, Ser. A **240**, 599 (1948).

[15] The waiting time for a thermally activated jump accross a barrier of height $\delta(H)$ is usually taken as $\tau=\tau_0\exp(\delta(H)/k_BT)$, where τ_0 is an attempt time, typically of the order of 10^{-9} s. Therefore, $\delta(H)=k_BT\ln(\tau/\tau_0)$. Assuming that, at a field H, the barrier is overcome at the typical measurement time $\tau=1$ s, we have $\delta(H)\approx 20k_BT$. See for instance, H. Zeng *et al.*, J. Magn. Magn. Mater. **251**, 283 (2002).

[16] P. Hansen, C. Clausen, G. Much, M. Rosenkranz, and K. Witter, J. Appl. Phys. **66**, 756 (1989).

[17] G.S. Cargill, in *Magnetism and Magnetic Materials–1973*, edited by C.D. Graham, Jr. and J.J. Rhyne, AIP Conf. Proc. No. 18 (AIP, New York, 1974).

[18] R. Hasegawa, J. Appl. Phys. **45**, 3109 (1974).

[19] Y. Mimura, N. Imamura, T. Kobayashi, A. Okada, and Y. Kushiro, J. Appl. Phys. **49**, 1208 (1978).

[20] S. Mangin, F. Montaigne, C. Bellouard, and H. Fritzche, Appl. Phys. A: Mater. Sci. Process. **A74**, S631 (2002).

[21] C.L. Platt, A.E. Berkowitz, S. David, E.E. Fullerton, J.S. Jiang, and S.D. Bader, Appl. Phys. Lett. **79**, 3992 (2001).

[22] As a consequence, the fanning mode cannot be found using a simple one-dimensional micromagnetic model, as ours.

[23] K. Mibu, T. Nagahama, T. Shinjo, and T. Ono, Phys. Rev. B **58**, 6442 (1998).

[24] D. Mauri, H.C. Siegmann, P.S. Bagus, and E. Kay, J. Appl. Phys. **62**, 3047 (1987).

[25] R.L. Stamps, J. Phys. D **33**, R247 (2000), and references therein.